Chemical Science

ROYAL SOCIETY OF CHEMISTRY

EDGE ARTICLE

View Article Online
View Journal | View Issue

Cite this: *Chem. Sci.*, 2026, **17**, 7064

All publication charges for this article have been paid for by the Royal Society of Chemistry

A chiral co-assembled exciplex host achieved extremely outstanding narrowband circularly polarized electroluminescence

Chao Liu,[a] Jun Zeng,[a] Zhenhao Jiang,[a] Yihan Chen,*[b] Junsheng Zhang*[a] and Yixiang Cheng *[a]

Received 10th December 2025
Accepted 9th February 2026

DOI: 10.1039/d5sc09684g

rsc.li/chemical-science

High-performance circularly polarized organic light-emitting diodes (CP-OLEDs) that can simultaneously achieve narrowband emission and high electroluminescence asymmetry factor (g_{EL}) values remain a formidable challenge. In this study, a simple strategy utilizing a co-assembled chiral exciplex as a host material was employed to fabricate high-performance CP-OLEDs. The exciplex was constructed from chiral acceptor enantiomers (*R*/*S*-TRZ) and an achiral liquid-crystalline donor (CzTPA). Upon thermal annealing, the resulting co-assembled films exhibited circularly polarized luminescence (CPL) with a luminescence asymmetry factor (g_{lum}) up to 0.58. Introducing the achiral green multiple-resonance thermally activated delayed fluorescence (MR-TADF) emitter to the exciplex host enabled high-performance circularly polarized electroluminescence (CP-EL). The resulting device exhibited a large g_{EL} value of 0.28, a narrow full width at half-maximum (FWHM) of 33 nm, and negligible efficiency roll-off. This work describes the first case of narrowband CP-OLEDs based on chiral co-assembled exciplex host materials, representing one of the highest g_{EL} values of reported narrowband emission CP-OLEDs to date. It further establishes a general strategy for fabricating high-performance CP-OLEDs with readily available achiral emitters, thereby significantly broadening applications in chiral optoelectronics.

Introduction

Recently, circularly polarized organic light-emitting diodes (CP-OLEDs) have attracted widespread attention due to their capability for direct circularly polarized light emission for 3D displays and next-generation lighting sources.[1–4] Since the first case of CP-OLEDs in 1997,[5] various device emitting layers (EMLs) have been explored, such as chiral organic small molecules,[6,7] chiral polymers,[8] chiral thermally activated delayed fluorescence (TADF) dyes,[9,10] chiral metal-complexes,[11,12] and so on.[13,14] However, most of the reported CP-OLEDs have exhibited low electroluminescence asymmetry factor (g_{EL}) values in the range of 10^{-5} to 10^{-3}, thereby largely limiting their application prospects.[15–17] In recent years, the chiral supramolecular assembly strategy has emerged as a promising and efficient strategy for developing high-performance CP-OLEDs.[18–22] Our group reported a series of CP-OLEDs with g_{EL} values of 10^{-2} order of magnitude based on chiral co-assembled EMLs.[23–26] Nevertheless, further increasing g_{EL} remains challenging and is critical for advancing high-performance CP-OLEDs.

Chiral multiple-resonance TADF (MR-TADF) molecules have emerged as the ideal emitters for high-performance CP-OLEDs owing to their high color purity and narrow emission.[27–30] However, the prolonged delayed fluorescence characteristic of MR-TADF emitters promotes exciton annihilation, which often results in severe efficiency roll-off and shortened operational lifetime in OLED devices.[31,32] An exciplex is an intermolecular charge transfer state emission, generated by a completely spatially separated donor–acceptor (D–A) molecular pair.[33,34] The physically blended D–A molecules can realize balanced and barrier-free charge transport, along with a more efficient reverse intersystem crossing (RISC).[35–37] These properties endow the exciplex with significant potential as a host for MR-TADF emitters, facilitating efficient Förster resonance energy transfer (FRET) of excitons to the emitters, and suppress efficiency roll-off of the MR-TADF OLEDs.[38–41] Additionally, an exciplex system featuring separated frontier orbitals would be favorable for a small electric transition dipole moment (μ), a large cos θ (θ is the angle between the magnetic transition dipole moment (m) and μ). This is conducive to the preparation of CP-OLED devices with large g values.[42] In 2022, Yang *et al.*[43] reported a chiral exciplex host formed by a chiral donor and an achiral acceptor, which sensitized an MR-TADF emitter *via* efficient FRET, achieving CP electroluminescence (CP-EL) with $|g_{EL}|$ of 2.8 ×

[a]*State Key Laboratory of Analytical Chemistry for Life Sciences, Engineering Research Center of Photoresist Materials, Ministry of Education, School of Chemistry and Chemical Engineering, Nanjing University, 163 Xianlin Avenue, Nanjing 210023, P.R. China. E-mail: zhangjs@nju.edu.cn; yxcheng@nju.edu.cn*

[b]*School of Chemistry and Materials Science, Jiangsu Normal University, Xuzhou 221116, P.R. China. E-mail: 6020240050@jsnu.edu.cn*

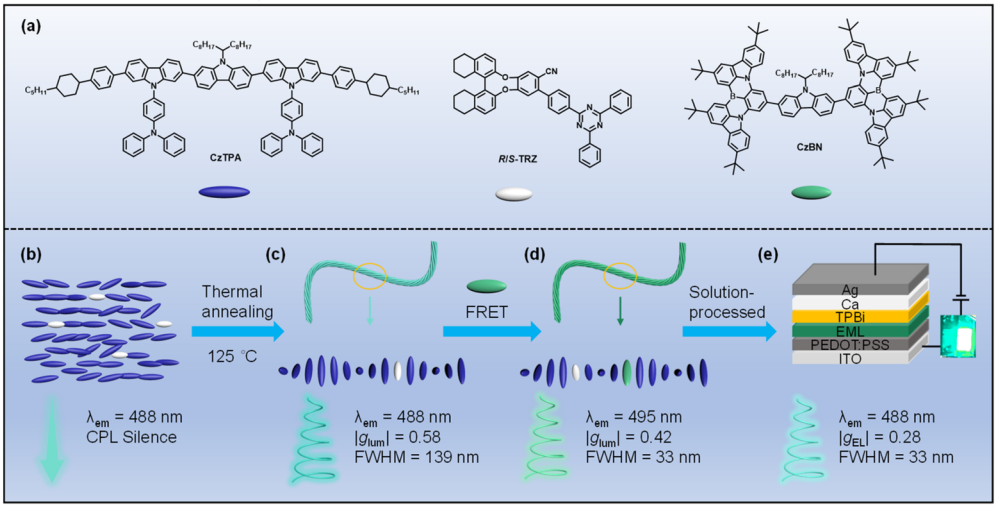

Scheme 1 (a) Chemical structures of CzTPA, *R*/*S*-TRZ, and CzBN; schematic diagram of the chiral co-assembled process, (b) before and (c) after thermal annealing, and (d) FRET process; (e) the device configuration of CP-OLEDs.

10^{-3} and narrow emission. In 2025, He *et al.*[42] developed a pair of triptycene-bridged enantiomers. When combined with PO-T2T to form a chiral host, the resulting CP-OLEDs exhibited an enhanced $|g_{EL}|$ value of 2.19×10^{-2}. The chiral exciplex host strategy provides a general approach for directly generating high-performance CP-EL. However, this strategy usually suffers from inherently low g_{EL} values, which continues to limit device performance.

In this work, we propose an effective strategy for constructing EMLs that yield CP-OLEDs with large g_{EL} values and narrowband emission. The approach employs a chiral co-assembled exciplex host, formed by doping an achiral liquid crystalline donor with a chiral acceptor, together with an achiral MR-TADF emitter, CzBN.[44] Specifically, the liquid crystalline molecule CzTPA was designed as a strong electron-donating unit, while axially chiral binaphthyl derivatives functionalized with a 2,4,6-triphenyl-1,3,5-triazine moiety (*R*/*S*-TRZ) served as chiral electron-accepting components (Scheme 1a). Then, chiral co-assembled exciplexes $(CzTPA)_{0.92}$-$(R/S\text{-}TRZ)_{0.08}$ were prepared by doping chiral inducers *R*/*S*-TRZ into the achiral liquid crystalline molecules CzTPA (Scheme 1b). After thermal annealing at 125 °C, the $(CzTPA)_{0.92}$-$(R/S\text{-}TRZ)_{0.08}$ films showed the strongest CPL emission ($|g_{lum}| = 0.58$, $\Phi_{FL} = 34.47\%$) due to the formation of regular helical nanofibers (Scheme 1c). Inspiringly, introducing an MR-TADF emitter into a chiral co-assembled exciplex host, the ternary co-assemblies showed strong CPL emission with a small full-width at half-maximum ($|g_{lum}| = 0.42$, FWHM = 33 nm) *via* a FRET mechanism (Scheme 1d). Furthermore, solution-processed CP-OLEDs employing the ternary co-assemblies as the EMLs achieved CP-EL with an FWHM of 33 nm, a maximum external quantum efficiency (EQE_{max}) of 2.0%, and g_{EL} of 0.28 (Scheme 1e). To the best of our knowledge, this work is the first case of narrowband CP-OLEDs based on chiral co-assembled exciplex host materials. Notably, this work can provide an efficient strategy for achieving high-performance CP-EL with narrowband emission from achiral emitters *via* a chiral co-assembled and energy transfer process.

Results and discussion

Synthesis and characterization

The synthetic procedures and detailed characterization data for CzTPA and *R*/*S*-TRZ are provided in the SI. Thermogravimetric analysis (TGA) and differential scanning calorimetry (DSC) were used to evaluate their thermal properties. As shown in Fig. S1a, CzTPA and *S*-TRZ exhibited excellent thermal stability with decomposition temperatures (T_d, 5% weight loss) of 479 and 472 °C, respectively, indicating that all compounds are essential for potential applications of high-performance OLEDs.[45–47] Subsequently, DSC was employed to investigate the phase transitions. For *S*-TRZ, only the melting temperature (T_m) of 176 °C was observed. But CzTPA exhibited temperature-dependent phase transition characteristics. The DSC curve of CzTPA showed T_m of 113 °C and isotropic temperatures (T_i) of 186 °C (Fig. S1b). Moreover, the temperature-dependent phase transition characteristics were further characterized using polarized optical microscopy (POM) and small angle X-ray scattering (SAXS). As shown in Fig. S2a, a clear threadlike texture was observed upon the heating process, indicating its nematic nature. Furthermore, a weak peak of SAXS profiles at $2\theta \approx 4.3°$ exhibited the nematic ordering peak, and the weak broad peak at $2\theta \approx 19°$ further confirmed the presence of a nematic liquid crystalline phase (Fig. S3a).

Electrochemical properties

Subsequently, the electrochemical properties of CzTPA and *S*-TRZ were evaluated by cyclic voltammetry (CV), and the results are summarized in Fig. S4 and Table S1. According to the absorption edge (λ_{onset}) and energy level gap (E_g), the highest occupied molecular orbital (HOMO) and lowest unoccupied molecular orbital (LUMO) energy levels of CzTPA and *S*-TRZ

were calculated to be −4.97/−1.13 eV and −6.19/−1.97 eV, respectively, which indicate that CzTPA can form an exciplex with *S*-TRZ. In addition, density functional theory (DFT) calculations on the models of CzTPA and *S*-TRZ were also performed. As shown in Fig. 1, the HOMO of CzTPA is almost completely distributed on the carbazole fragments, while the LUMO of *S*-TRZ is almost completely distributed on the triphenyltriazine fragment, which indicates efficient charge transfer interactions from CzTPA to *S*-TRZ.[48] And the theoretically calculated HOMO/LUMO energy levels of CzTPA and *S*-TRZ were located at −4.99/−1.20 eV and −6.23/−1.97 eV, respectively, which were in good agreement with the CV experimental data.

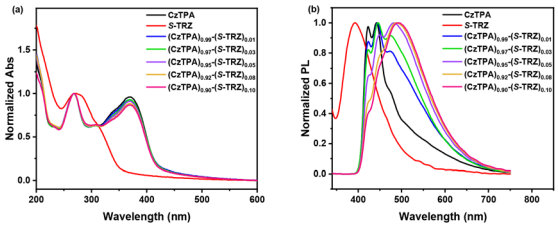

Fig. 2 (a) UV-vis absorption and (b) PL spectra of CzTPA, *S*-TRZ, and $(CzTPA)_x$-$(S\text{-}TRZ)_y$ in spin-coated films after thermal annealing.

Photophysical properties

The UV-vis absorption and photoluminescence (PL) spectra of CzTPA and *S*-TRZ were measured in spin-coated films. The absorption band of CzTPA at 268 nm corresponds to the π–π* transition of the carbazole moiety, whereas the absorption at 368 nm arises from the extended π-conjugated structure. For *S*-TRZ, the absorption maximum at 269 nm is also attributed to π–π* transitions (Fig. 2a). The PL emission peaks of CzTPA were located at 423 and 442 nm, while *S*-TRZ showed a single emission peak at 393 nm. In order to achieve CPL emission, co-assembled films $(CzTPA)_x$-$(S\text{-}TRZ)_y$ were prepared by blending achiral CzTPA with varying weight percentages (wt%) of chiral *S*-TRZ. Intriguingly, the absorption spectrum of $(CzTPA)_x$-$(S\text{-}TRZ)_y$ was a simple overlap of the two components of CzTPA and *S*-TRZ, indicating that there was no formation of charge-transfer complexes in the ground state.[49] Compared with the CzTPA and *S*-TRZ, $(CzTPA)_x$-$(S\text{-}TRZ)_y$ exhibited a significantly red-shifted emission, which indicated the formation of exciplexes upon optical excitation.[50] To further investigate the photophysical properties of exciplexes, the transient photoluminescence decay profiles were measured.[51] As the wt% of *S*-TRZ increased to 10%, $(CzTPA)_x$-$(S\text{-}TRZ)_y$ displayed a significantly increased fluorescence lifetime from 0.74 to 98.80 ns. The results and photoluminescence quantum yields (PLQY) are summarized in Fig. S5 and Table S2.

Chiroptical properties

The chiroptical properties of the *R*/*S*-TRZ and $(CzTPA)_x$-$(R/S\text{-}TRZ)_y$ in spin-coated films were investigated using circular dichroism (CD) and CPL spectra. As shown in Fig. S6a, *R*/*S*-TRZ exhibited good mirrored CD signals in the 200–350 nm range. However, no CPL signals were detected (Fig. S6b). Meanwhile, the films of $(CzTPA)_x$-$(R/S\text{-}TRZ)_y$ exhibited weak mirror-imaged CD bands with the new Cotton effect bands and CPL signals before thermal annealing (Fig. S6c and d). Based on the CPL spectra of co-assembled $(CzTPA)_{0.92}$-$(S\text{-}TRZ)_{0.08}$ films annealed at different temperatures (Fig. S7a), the optimal annealing temperature was determined to be 125 °C. After annealing at 125 °C for 20 min, both CD and CPL signals of $(CzTPA)_x$-$(R/S\text{-}TRZ)_y$ were significantly enhanced (Fig. 3a and b), which indicated that the thermal annealing treatment process promoted the formation of chiral co-assemblies with a highly regular arrangement.[52] Among the tested compositions, the films with 8 wt% *R*/*S*-TRZ doping showed the strongest Cotton effect peaks at 378 nm and CPL emissions at 488 nm ($|g_{lum}| = 0.58$) (Fig. S7b). Based on the above data, $(CzTPA)_{0.92}$-$(R/S\text{-}TRZ)_{0.08}$ can be selected as the chiral co-assembled exciplex host for making high-performance CP-OLEDs.

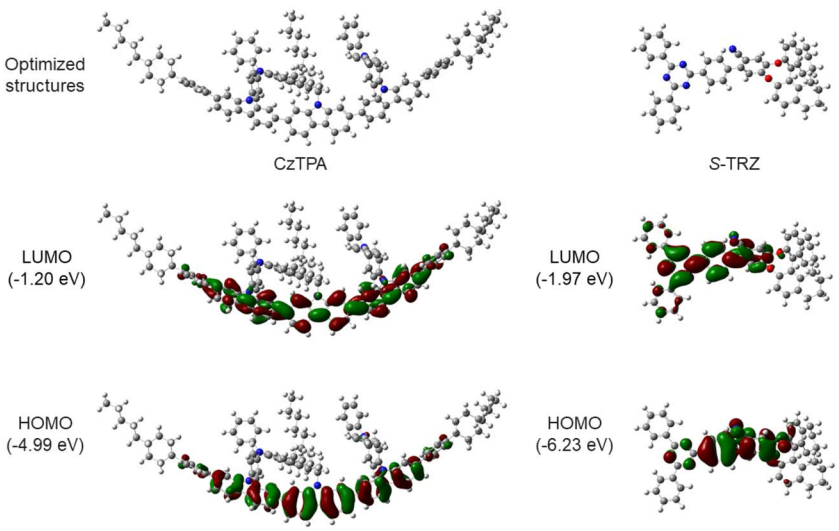

Fig. 1 Optimized structures and calculated HOMO–LUMO spatial distributions of CzTPA and *S*-TRZ.

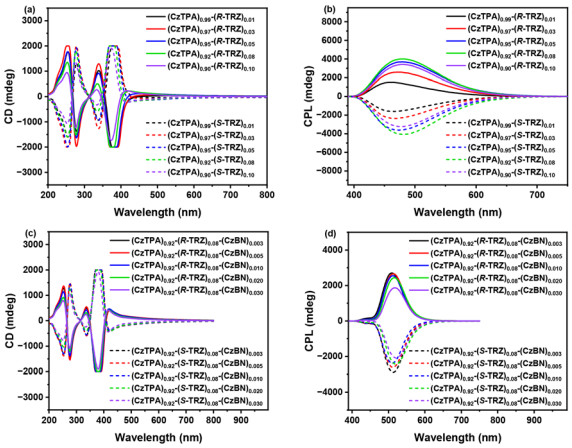

Fig. 3 CD spectra of (a) $(CzTPA)_x$-$(R/S\text{-}TRZ)_y$ and (c) $(CzTPA)_{0.92}$-$(R/S\text{-}TRZ)_{0.08}$-$(CzBN)_z$; CPL spectra of (b) $(CzTPA)_x$-$(R/S\text{-}TRZ)_y$ and (d) $(CzTPA)_{0.92}$-$(R/S\text{-}TRZ)_{0.08}$-$(CzBN)_z$ in spin-coated films.

To achieve high performance CP-OLEDs that combine large g_{EL} values and narrowband emission, chiral co-assembled exciplexes $(CzTPA)_{0.92}$-$(R/S\text{-}TRZ)_{0.08}$ were selected as both the host and energy donor, while the MR-TADF molecule CzBN, known for its narrowband emission, served as the energy acceptor for FRET. As illustrated of Fig. S8a, the absorption spectrum of CzBN overlaps strongly with the PL of $(CzTPA)_{0.92}$-$(S\text{-}TRZ)_{0.08}$ over the 387–501 nm range, suggesting that efficient FRET can occur from the exciplex host to CzBN upon photoexcitation. Subsequently, a series of ternary chiral co-assemblies were fabricated by doping different wt% of CzBN into $(CzTPA)_{0.92}$-$(S\text{-}TRZ)_{0.08}$. These ternary chiral co-assembled films of $(CzTPA)_{0.92}$-$(S\text{-}TRZ)_{0.08}$-$(CzBN)_z$ displayed narrowband emission in the range of 495–500 nm and FWHMs of 33–37 nm, respectively (Fig. S8b and Table S3). Intriguingly, narrowband emission was preserved even at a low doping ratio of 0.3 wt%. In addition to narrowing the emission peak, the PLQY of ternary chiral co-assembled films was also significantly enhanced. The PLQY of $(CzTPA)_{0.92}$-$(S\text{-}TRZ)_{0.08}$ was only 34.47%, and that of $(CzTPA)_{0.92}$-$(S\text{-}TRZ)_{0.08}$-$(CzBN)_{0.003}$ was increased to 68.82%. The fluorescence lifetime and PLQY are summarized in Fig. S9 and Table S3.

The CD and CPL spectra of $(CzTPA)_{0.92}$-$(R/S\text{-}TRZ)_{0.08}$-$(CzBN)_z$ were further investigated. Before thermal annealing, the ternary co-assembled films displayed very weak CD signals, similar to films of $(CzTPA)_{0.92}$-$(R/S\text{-}TRZ)_{0.08}$ (Fig. S10a). After thermal annealing at 125 °C for 20 min, these films exhibited an obvious doping ratio dependence behavior and enhanced CD signals. With the increase of doped CzBN from 0.3 to 2.0 wt%, the strongest cotton effect peaks at 373 nm decreased, suggesting that excess of CzBN disrupts the chiral co-assembled process (Fig. 3c).[53] Corresponding CPL spectra revealed a similar trend: the as-prepared films displayed weak CPL emission (Fig. S10b), whereas after annealing, the optimized $(CzTPA)_{0.92}$-$(R/S\text{-}TRZ)_{0.08}$-$(CzBN)_{0.003}$ film exhibited a strong CPL signal at 495 nm with $|g_{lum}|$ of 0.42 (Fig. 3d and S10c).

Morphology study

To deeply understand the chiral transfer and induction mechanism, the morphological evolution of $(CzTPA)_{0.92}$-$(S\text{-}TRZ)_{0.08}$ and $(CzTPA)_{0.92}$-$(S\text{-}TRZ)_{0.08}$-$(CzBN)_{0.003}$ under different conditions was measured using scanning electron microscopy (SEM). The spin-coated films of all materials exhibited smooth surfaces both before and after thermal annealing (Fig. 4a, d and S11a, d). To better visualize the co-assembly behavior, diluted films (0.2 mg mL^{-1} in toluene) and the aggregated states (2×10^{-3} mg mL^{-1} in THF/H_2O = 60/40, v/v) were prepared. SEM images of the diluted films revealed the emergence of ordered morphologies after thermal annealing, which were not apparent in the before thermal annealing samples (Fig. 4b, e and S11b, e). Notably, compared with the aggregates before thermal annealing (Fig. S11c and f), the aggregates after thermal annealing formed highly regular left-handed helix (*M*-helix) nanofibers (Fig. 4c and f), consistent with the significant enhancement of CD and CPL signals. Furthermore, SAXS profiles confirmed that the chiral co-assemblies develop a well-ordered helical superstructure, characteristic of a chiral nematic liquid crystalline phase (Fig. S3b and c).[54,55]

CP-EL properties

The film-forming properties of the EMLs are crucial for achieving high-performance OLEDs. The surface morphologies of the spin-coated films of $(CzTPA)_{0.92}$-$(S\text{-}TRZ)_{0.08}$ and $(CzTPA)_{0.92}$-$(S\text{-}TRZ)_{0.08}$-$(CzBN)_{0.03}$ were probed by atomic force microscopy (AFM). As shown in Fig. S12, the AFM images of films annealed at 125 °C reveal smooth and homogeneous surfaces, with root-mean-square (RMS) roughness values as low as 0.22 nm for both compositions. The absence of particle aggregation or phase separation further confirms their excellent film-forming ability. These results demonstrate that such chiral co-assemblies are suitable for use as EMLs in CP-OLEDs.[56,57] Subsequently, the EL performances of *R*/*S*-D devices based on $(CzTPA)_{0.92}$-$(R/S\text{-}TRZ)_{0.08}$-$(CzBN)_{0.03}$ were investigated. Solution-processed CP-OLEDs were constructed with the following architecture: indium tin oxide (ITO)/poly(3,4-ethylenedioxythiophene): poly(styrenesulfonate) (PEDOT:PSS) (25 nm, hole-injection layer)/$(CzTPA)_{0.92}$-$(R/S\text{-}TRZ)_{0.08}$-

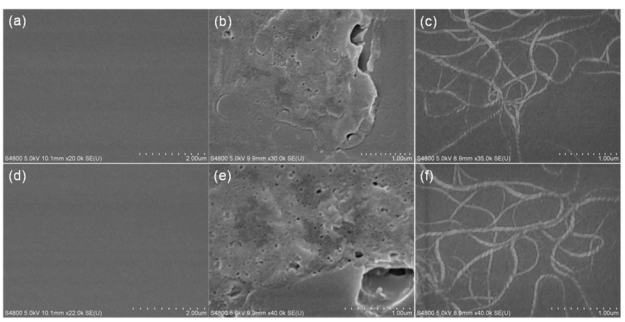

Fig. 4 SEM images of (a–c) $(CzTPA)_{0.92}$-$(S\text{-}TRZ)_{0.08}$ and (d–f) $(CzTPA)_{0.92}$-$(S\text{-}TRZ)_{0.08}$-$(CzBN)_{0.003}$ after thermal annealing ((a and d): film, 20 mg mL^{-1} in toluene; (b and e): film, 0.2 mg mL^{-1} in toluene; (c and f): aggregate state, 2×10^{-3} mg mL^{-1} in THF/H_2O = 60/40, v/v).

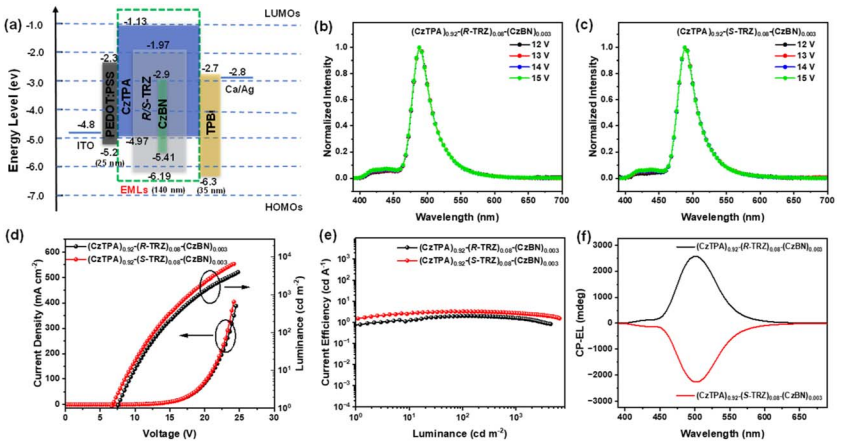

Fig. 5 (a) The energy level diagram; EL spectra of the devices: (b) *R*-D and (c) *S*-D; (d) *J*–*V*–*L* curves; (e) CE–*L* curves; (f) CP-EL spectra of the *R*/*S*-D devices.

$(CzBN)_{0.003}$ (140 nm, EML)/TPBi (35 nm, electron-transport layer)/Ca (10 nm)/Ag (100 nm). The energy levels of the devices, EL spectra, current density–voltage–luminance (*J*–*V*–*L*), current efficiency–luminance (CE–*L*) characteristics and CP-EL spectra are depicted in Fig. 5. All the characteristics of devices are listed in Table S4. As a result, after the thermal annealing process of EMLs, the *R*/*S*-D displayed a green narrowband emission (λ_{EL} = 488 nm, FWHM = 33 nm) with CIE coordinates of [0.13, 0.38]. Additionally, *R*/*S*-D exhibited commendable device performances with turn-on voltages (V_{on}) of 7.5/6.6 V, high maximum luminance (L_{max}) of 4376/6471 cd m^{-2}, maximum current efficiencies (CE_{max}) of 2.1/3.4 cd A^{-1}, and EQE_{max} of 1.2%/2.0%. Furthermore, a low efficiency roll-off was achieved, with the device retaining an EQE of 1.0%/1.7% at 1000 cd m^{-2}, demonstrating the advantage of the exciplex host in minimizing efficiency loss at high luminance for efficient CP-OLEDs. Importantly, their CP-EL performances were also evaluated, and the device displayed strong CP-EL signals with high g_{EL} values of up to +0.28/−0.27 (λ_{em} = 488 nm) (Fig. S13), representing one of the highest g_{EL} values of the reported narrowband emission CP-OLEDs to date (Table S5). These results verify the effectiveness of the co-assembled exciplex host strategy for highly efficient CP-OLEDs with narrowband emission and large g_{EL} values.

Conclusions

In summary, chiral exciplex host systems were successfully constructed through the co-assembly of a chiral acceptor (*R*/*S*-TRZ) and an achiral liquid-crystalline donor (CzTPA). By introducing an MR-TADF emitter into these hosts, ternary co-assemblies were obtained that exhibited strong CPL with $|g_{lum}|$ up to 0.42 arising from their well-defined helical nanofiber morphology. Most importantly, these ternary co-assemblies were successfully employed as the EMLs of solution-processed CP-OLEDs. The devices achieved CP-EL with FWHM = 33 nm, EQE_{max} of 2.0%, and $|g_{EL}|$ of 0.28. This study provides a simple and general strategy for designing nearly roll-off-free and high g_{EL} CP-EL materials with narrowband emission using a co-assembled chiral exciplex-forming co-host. We believe that a multi-component co-assembled chiral functional layer might serve as an ideal platform for high-performance CP-OLEDs.

Author contributions

C. Liu: formal analysis, investigation, methodology, writing – original draft; J. Zeng: formal analysis, investigation, methodology; Z. Jiang: investigation; Y. Chen: formal analysis, investigation; J. Zhang: supervision, investigation; Y. Cheng: conceptualization, funding acquisition, supervision, writing – review and editing.

Conflicts of interest

There are no conflicts to declare.

Data availability

The data supporting this article have been included as part of the supplementary information (SI). Supplementary information: materials and measurements, experimental details, spectral data and additional data. See DOI: https://doi.org/10.1039/d5sc09684g.

Acknowledgements

This work was supported by the National Natural Science Foundation of China (92156014, 52373188).

References

1 D.-W. Zhang, M. Li and C.-F. Chen, *Chem. Soc. Rev.*, 2020, **49**, 1331–1343.
2 Y.-H. Kim, Y. Zhai, H. Lu, X. Pan, C. Xiao, E. A. Gaulding, S. P. Harvey, J. J. Berry, Z. V. Vardeny, J. M. Luther and M. C. Beard, *Science*, 2021, **371**, 1129–1133.
3 A. Ren, H. Wang, W. Zhang, J. Wu, Z. Wang, R. V. Penty and I. H. White, *Nat. Electron.*, 2021, **4**, 559–572.

4 F. Furlan, J. M. Moreno-Naranjo, N. Gasparini, S. Feldmann, J. Wade and M. J. Fuchter, *Nat. Photon.*, 2024, **18**, 658–668.
5 E. Peeters, M. P. T. Christiaans, R. A. J. Janssen, H. F. M. Schoo, H. P. J. M. Dekkers and E. W. Meijer, *J. Am. Chem. Soc.*, 1997, **119**, 9909–9910.
6 A. Altinier, E. Machalska, I. Fortunati, I. Fortunati, M. Raulin, C. Zonta, G. Mazzeo, G. Longhi, M. Fusè, K. Wurst, S. Veglianti, L. D. Vico and D. Padula, *J. Am. Chem. Soc.*, 2025, **147**, 32357–32364.
7 Y. Yan, Z. Cheng, Y. Xu, Z. Su, Y. Wang, X. He, Z. Zhao, F. Liu and P. Lu, *Adv. Funct. Mater.*, 2024, **34**, 2408550.
8 K.-K. Tan, W.-C. Guo, W.-L. Zhao, M. Li and C.-F. Chen, *Angew. Chem., Int. Ed.*, 2024, **63**, e202412283.
9 R. Chowdhury, M. D. Preuss, H.-H. Cho, J. J. P. Thompson, S. Sen, T. K. Baikie, P. Ghosh, Y. Boeije, X. W. Chua, K.-W. Chang, E. Guo, J. van der Tol, B. W. L. van den Bersselaar, A. Taddeucci, N. Daub, D. M. Dekker, S. T. Keene, G. Vantomme, B. Ehrler, S. C. J. Meskers, A. Rao, B. Monserrat, E. W. Meijer and R. H. Friend, *Science*, 2025, **387**, 1175–1181.
10 N. Su, J. Wang, Y. Yang, Z. Yan, L. Zhou, Y.-X. Zheng and J. Ding, *Angew. Chem., Int. Ed.*, 2025, **64**, e202512717.
11 M. Y. Petyuk, L. Meng, Z. Ma, A. M. Agafontsev, I. Y. Bagryanskaya, A. S. Berezin, J. Zhang, A. Chu, M. I. Rakhmanova, H. Meng, A. V. Tkachev, V. W.-W. Yam and A. V. Artem'ev, *Angew. Chem., Int. Ed.*, 2024, **63**, e20241243.
12 M. P. Davydova, T. Xu, A. M. Agafontsev, L. Meng, M. Wolff, M. Y. Petyuk, I. Y. Bagryanskaya, A. S. Berezin, A. V. Tkachev, H. Meng and A. V. Artem'ev, *Angew. Chem., Int. Ed.*, 2025, **64**, e202419788.
13 X.-Y. Ding, L.-X. Shi, J.-Y. Wang, L.-J. Xu, L.-Y. Zhang and Z.-N. Chen, *Angew. Chem., Int. Ed.*, 2025, **64**, e202417934.
14 F. Zheng, X.-L. Liu, L. Xing, J.-M. Jin, S. Ji, Y. Huo and W.-C. Chen, *Angew. Chem., Int. Ed.*, 2025, **64**, e202504057.
15 Y. Yang, N. Li, J. Miao, X. Cao, A. Ying, K. Pan, X. Lv, F. Ni, Z. Huang, S. Gong and C. Yang, *Angew. Chem., Int. Ed.*, 2022, **61**, e202202227.
16 X. Cai, J. Wei, Z. Li, Y. Pu, Y. Wu and Y. Wang, *Chem. Sci.*, 2025, **16**, 11539–11547.
17 L. Chen, P. Zou, J. Chen, L. Xu, B. Z. Tang and Z. Zhao, *Nat. Commun.*, 2025, **16**, 1656.
18 M. Liu, L. Zhang and T. Wang, *Chem. Rev.*, 2015, **115**, 7304–7397.
19 Z. L. Gong, X. Zhu, Z. Zhou, S. W. Zhang, D. Yang, B. Zhao, Y. P. Zhang, J. Deng, Y. Cheng, Y. X. Zheng, S. Q. Zang, H. Kuang, P. Duan, M. Yuan, C. F. Chen, Y. S. Zhao, Y. W. Zhong, B. Z. Tang and M. Liu, *Sci. China Chem.*, 2021, **64**, 2060–2104.
20 Y. Zhang, W. Yu, H. Li, W. Zheng and Y. Cheng, *Chem. Eur. J.*, 2023, **29**, e202204039.
21 C.-H. Guo, L. Feng, C.-F. Chen and M. Li, *Angew. Chem., Int. Ed.*, 2025, **64**, e202516018.
22 Z.-X. Yu, X.-W. Chen, C.-F. Chen and M. Li, *Angew. Chem., Int. Ed.*, 2025, e202517906.
23 Y. Zhang, Y. Li, Y. Quan, S. Ye and Y. Cheng, *Angew. Chem., Int. Ed.*, 2023, **62**, e202214424.
24 Z. Geng, Z. Liu, H. Li, Y. Zhang, W. Zheng, Y. Quan and Y. Cheng, *Adv. Mater.*, 2023, **35**, 2209495.
25 Y. Zhang, D. Li, Q. Li, Y. Quan and Y. Cheng, *Adv. Funct. Mater.*, 2023, **33**, 2309133.
26 C. Fu, D. Li, C. Liu, Y. Zhang, J. Zhang and Y. Cheng, *Angew. Chem., Int. Ed.*, 2025, **64**, e202512257.
27 C. Shi, J.-M. Jin, R.-J. Wang, W.-C. Chen, C.-L. Sun, S. Ji, Y. Huo and H.-L. Zhang, *Adv. Mater.*, 2025, **37**, 2420611.
28 X.-S. Zhong, J.-Q. Xi, Z.-P. Yan, J.-J. Hu, Y. Wang, L. Yuan, S.-Q. Song, J.-L. Zuo and Y.-X. Zheng, *Adv. Funct. Mater.*, 2025, **35**, 2504525.
29 L. Li, Y. Xu, Y. Sun, Y. Qu, W. Cui, L. Guo, P. Zheng, Y. Wang and C. Li, *Adv. Mater.*, 2025, e11560.
30 Z. Yan, J. Lin, Q. Chen, X. Zhuang, L. Yuan, Z. Li, Z. Wang, Y.-X. Zheng, Y. Wang and H. Bi, *Adv. Mater.*, 2025, e11230.
31 Y. Kondo, K. Yoshiura, S. Kitera, H. Nishi, S. Oda, H. Gotoh, Y. Sasada, M. Yanai and T. Hatakeyama, *Nat. Photon.*, 2019, **13**, 678–682.
32 M. Yang, I. Park and T. Yasuda, *J. Am. Chem. Soc.*, 2020, **142**, 19468–19472.
33 X.-K. Liu, Z. Chen, C.-J. Zheng, C.-L. Liu, C.-S. Lee, F. Li, X.-M. Ou and X.-H. Zhang, *Adv. Mater.*, 2015, **27**, 2378–2383.
34 Y. Lee, H. Y. Kim, H. Kwak, C. Y. Park, S. Kwon, S. Kim, E. Lim, K. Jin, C. S. Hong, W.-S. Chae, M. Han, M. J. Cho, S. Park and D. H. Choi, *Adv. Funct. Mater.*, 2025, e13345.
35 Q. Wang, Q.-S. Tian, Y.-L. Zhang, X. Tang and L.-S. Liao, *J. Mater. Chem. C*, 2019, **7**, 11329–11360.
36 M. Zhang, C.-J. Zheng, H. Lin and S.-L. Tao, *Mater. Horiz.*, 2021, **8**, 401–425.
37 Z. Wang, T. Li, Y. Song, D. Zhuang, S. Yang and L. He, *Chem. Sci.*, 2025, **16**, 21068–21078.
38 T. Nguyen, H. Nakanotani, T. Hatakeyama and C. Adachi, *Adv. Mater.*, 2020, **32**, 1906614.
39 X. Lu, Q. Wang, X. Cai, Y. Qu, Z. Li, C. Li and Y. Wang, *Adv. Funct. Mater.*, 2024, **34**, 2313897.
40 D. Liu, G.-X. Yang, Z. Chen, W. Xie, D. Li, W. Li, J. Lin, X. Nie, Z. Li, B. Liang, Z. Yang, Z. Wang, J. Pu, G. Sun, C. Shen, M. Li and S.-J. Su, *Adv. Mater.*, 2024, **36**, 2403584.
41 Y. Nie, C. Jiang, C. Cao, B. Liang, X. Zhuang, H. Bi and Y. Wang, *Adv. Funct. Mater.*, 2025, **35**, 2419495.
42 Y. Xie, S. Zeng, W. Huang, C. Wei and Z. He, *Angew. Chem., Int. Ed.*, 2025, **64**, e202511414.
43 Z. Chen, C. Zhong, J. Han, J. Miao, Y. Qi, Y. Zou, G. Xie, S. Gong and C. Yang, *Adv. Mater.*, 2022, **34**, 2109147.
44 T. Wang, X. Yin, X. Cao and C. Yang, *Angew. Chem., Int. Ed.*, 2023, **62**, e202301988.
45 X. L. Liu, L. Hua, X. Y. Lai, J. H. Kim, Q. Zhu, J. Y. Lee, W. G. Zhu and Y. F. Wang, *Adv. Mater.*, 2025, **37**, 2500690.
46 S. Debnath, P. Ramkissoon, U. Salzner, C. Hall, N. Panjwani, W. Kim, T. Smith and S. Patil, *Nat. Commun.*, 2025, **16**, 2982.
47 W. Xie, X. Cao, M. Huang, K. Xu, C. Gui, Z. X. Chen, X. Song, Y. Wei, H. Liu, T. Hua, M. Yang, X. Yin, J. S. Miao and C. L. Yang, *J. Am. Chem. Soc.*, 2025, **147**, 8178–8187.
48 C. Duan, C. Han, R. Du, Y. Wei and H. Xu, *Adv. Opt. Mater.*, 2018, **6**, 1800437.
49 M. Huang, B. Jiang, G. Xie and C. Yang, *J. Phys. Chem. Lett.*, 2017, **8**, 4967–4973.

50 Z. Chen, M. Huang, C. Zhong, X. Cao, G. Xie, S. Gong and C. Yang, *Adv. Funct. Mater.*, 2023, **33**, 2215179.
51 K. Goushi, K. Yoshida, K. Sato and C. Adachi, *Nat. Photonics*, 2012, **6**, 253–258.
52 Z. Geng, Y. Zhang, Y. Zhang, Y. Quan and Y. Cheng, *Angew. Chem., Int. Ed.*, 2022, **61**, e202202718.
53 H. Li, D. Li, Z. Jiang, Y. Wang and Y. Cheng, *Chem. Sci.*, 2025, **16**, 17487–17493.
54 C.-J. Yu, D.-M. Lee, J.-K. Han, Y.-J. Lee, S.-W. Kim, E. Choi and J.-H. Kim, *Adv. Opt. Mater.*, 2022, **10**, 2101674.
55 Q. Guo, M. Zhang, Z. Tong, S. Zhao, Y. Zhou, Y. Wang, S. Jin, J. Zhang, H. B. Yao, M. Zhu and T. Zhuang, *J. Am. Chem. Soc.*, 2023, **145**, 4246–4253.
56 S. Wu, D. Chen, X. H. Zhang, D. M. Sun and E. Zysman-Colmn, *Adv. Mater.*, 2025, **37**, 2415289.
57 K. Y. Zhang, X. D. Wang, M. Y. Wang, S. M. Wang and L. X. Wang, *Angew. Chem., Int. Ed.*, 2025, **64**, e202423812.